PERGAMON

International Journal of Solids and Structures 36 (1999) 4055–4070

INTERNATIONAL JOURNAL OF SOLIDS and STRUCTURES

Behaviors of a single crack in multiple bolted joints

S. H. Ju*, T. L. Horng

Department of Civil Engineering, National Cheng-Kung University, Tainan, Taiwan, R.O.C.

Received 4 June 1997; revised 5 June 1998

Abstract

This paper examines the pin load ratios and the stress intensity factors (SIFs) of a single crack in the multiple bolted joints by using finite element analyses. Cubic-spline contact elements and rigid links were used to model the contact surface between the bolt and the rigid pin. The least-squares method was used to determine the SIFs. The finite element results indicate that the cracked hole can still sustain the major part of the original loading at the uncracked condition. The first hole sustains the largest pin load and mode-I SIF, which are reduced little for crack propagation. This critical condition cannot be reduced by the arrangement of more pins in the plate. In this paper, two simple formulae were also investigated to fit the load ratios and SIFs of the multiple bolted-joints problems.

Keywords: Bolted joints; Cubic spline; Contact; Finite Element; Friction; Stress intensity factors

1. Introduction

Due to stress concentrations, cracks often exist around the hole boundary of bolted joints. Generally, it is necessary to determine the stress intensity factors (SIFs) in order to evaluate the crack growth, residual strength and fatigue life of cracked joints. The SIFs of the cracked plate containing single bolted joint were studied in these references (Smith et al., 1979; Cartwright and Ratcliffe, 1972; Hong and Chu, 1982; Kirkby and Rooke, 1977; Liu and Kan, 1977; Cartwright and Parker, 1982; Hsu, 1981; Chiang and Rowlands, 1991; Narayana et al., 1994; Ju, 1997a). The brief discussion of above references can be found in Ju's paper (Ju, 1997a). The experimental and numerical stress analyses of multiple bolted joints were investigated by Rahman and Rowlands (1993) and Griffin et al. (1994). However, the SIFs of the cracked plate containing multiple bolted joints appears to be absent in the literature.

This paper examines the SIFs of a single crack in the multiple bolted joints. A fine mesh was used between the contact surface and the crack tip in order to obtain an accurate solution. The cubic-spline contact elements enhanced from the node-to-line contact element (Ju et al., 1995)

* Corresponding author. Tel.: +886-6-2757575-63119; Fax: +886-6-2358542; E-mail: juju@mail.ncku.edu.tw

0020–7683/99/$ - see front matter
PII: S0020–7683(98)00190–5

were used to model the contact surface between the bolt and the rigid pin. Moreover, the least-squares method (Ju, 1996) was used to determine the SIFs.

2. Formulating cubic-spline contact element

The stiffness matrix and the internal force vector of the node-to-cubic-spline contact element are illustrated below.

2.1. Element stiffness matrix of the three-node contact element

Let df_s be the incremental nodal frictional force, and df_n be the incremental nodal normal force between two iterations, the sticking stiffness matrix at one point is

$$\begin{Bmatrix} df_s \\ df_n \end{Bmatrix} = \begin{bmatrix} k & 0 \\ 0 & k \end{bmatrix} \begin{Bmatrix} dU \\ dV \end{Bmatrix} = \mathbf{K} \begin{Bmatrix} dU \\ dV \end{Bmatrix} \tag{1}$$

dV and dU are the displacements in the normal and tangential directions between two iterations, and k is a penalty constant. The sliding element stiffness can be written as:

$$\begin{Bmatrix} df_s \\ df_n \end{Bmatrix} = \begin{bmatrix} 0 & \mu k \\ 0 & k \end{bmatrix} \begin{Bmatrix} dU \\ dV \end{Bmatrix} = \mathbf{K}_{pu} \begin{Bmatrix} dU \\ dV \end{Bmatrix} \tag{2}$$

μ is the frictional coefficient with the positive or negative sign, while μ is positive for $\Delta U < 0$ and negative for $\Delta U > 0$, and ΔU is the difference in the relative tangential displacement between the current time step and the previous time step. $\mathbf{K}_{pu}$ is unsymmetrical, and can be replaced by a symmetric stiffness matrix as follows:

$$\begin{Bmatrix} df_s \\ df_n \end{Bmatrix} = k \begin{bmatrix} \mu^2 & \mu \\ \mu & 1 \end{bmatrix} \begin{Bmatrix} dU \\ dV \end{Bmatrix} = \mathbf{K}_{ps} \begin{Bmatrix} dU \\ dV \end{Bmatrix} \tag{3}$$

Equation (3) obeys the Mohr-Coulomb friction theory ($df_s = \mu df_n$). If $\mu k dU$ in eqn (3) is omitted from the calculation of the total normal force ($F_n = kV$), the contact analyses from eqns (2) and (3) will produce the similar result at the convergent state ($dU \cong 0$ and $dV \cong 0$). Thus, a symmetric formulation can be obtained. When the contact node approaches to the correct location using a numerical iteration scheme. The two value dU and dV will approach to zero and this omitted term $\mu \mathbf{K} dU$ will also approach to zero. For a nonlinear problem by using the tangent stiffness method, the stiffness matrix is always an approximate guess matrix trying to approach to the correct solution. In frictional contact problems, the stiffness matrix should be unsymmetrical, so the memory and CPU time requirements are intense. Therefore, choosing a symmetric formulation might be alternative.

The local stiffness matrices ($\mathbf{K}_{local} = \mathbf{K}$, $\mathbf{K}_{pu}$ or $\mathbf{K}_{ps}$) shown in eqns (1–3) must be transformed into the global coordinates as follows:

$$\mathbf{K}_{global} = \begin{bmatrix} \cos\theta & \sin\theta \\ -\sin\theta & \cos\theta \end{bmatrix}^T \mathbf{K}_{local} \begin{bmatrix} \cos\theta & \sin\theta \\ -\sin\theta & \cos\theta \end{bmatrix} \tag{4}$$

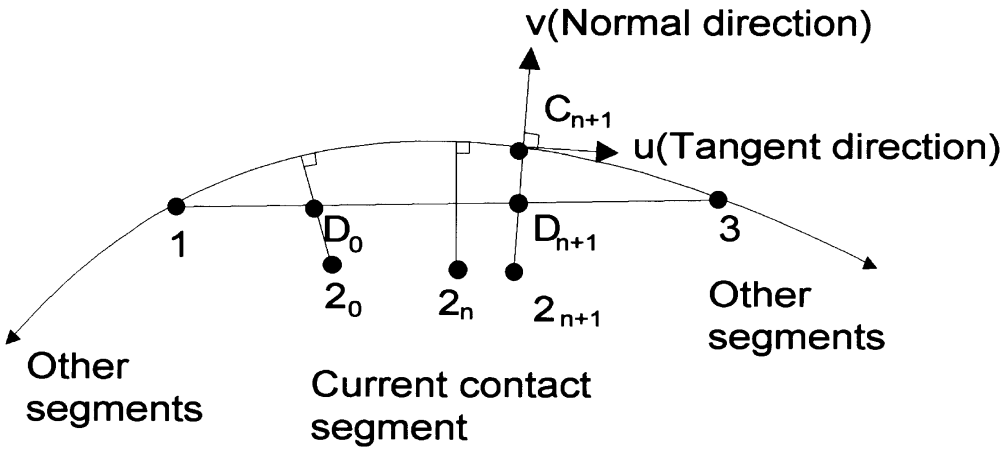

1 and 3 =The two edge nodes of the active segment of the cubic spline
2_0 = Node 2 at last time (force) step at the convergent state
2_n = Node 2 at this time (force) step and last iteration (iteration n)
2_{n+1} = Node 2 at this time (force) step and this iteration (iteration n+1)
C_{n+1} = Contact node on the cubic spline at this time (force) step and this iteration
D_0 = Contact node on line 1-3 at last time (force) step at the convergent state
D_{n+1} = Contact node on line 1-3 at this time (force) step and this iteration
u = Tangent direction at contact node C_{n+1}
v = Normal direction at contact node C_{n+1}

Fig. 1. Contact conditions between two force steps and two iterations.

where cos θ and sin θ are the components of the tangent direction (**u**) at the current contact node (C_{n+1}) in Fig. 1. This tangent direction (**u**) is always continuous along these cubic splines generated from the target nodes.

From Fig. 1, the nodal forces in the global directions for nodes 1, 2_{n+1} and 3, ($\mathbf{f}_1$, $\mathbf{f}_2$ and $\mathbf{f}_3$) are

$$\begin{Bmatrix}\mathbf{f}_1\\ \mathbf{f}_2\\ \mathbf{f}_3\end{Bmatrix} = \begin{bmatrix} s_n\begin{bmatrix}1 & 0\\ 0 & 1\end{bmatrix}\\ -\begin{bmatrix}1 & 0\\ 0 & 1\end{bmatrix}\\ s_m\begin{bmatrix}1 & 0\\ 0 & 1\end{bmatrix}\end{bmatrix}\mathbf{f}_c \quad \text{or} \quad \mathbf{f}=\mathbf{H}^T\mathbf{f}_c \tag{5}$$

where $\mathbf{f}_c$ is the nodal force vector of the contact node C_{n+1} in the global directions,

$$S_n = \frac{L_{D_{n+1}-3}}{L_{1-3}},$$

$S_m = 1 - S_n$, and L_{1-3} is the length between points 1 and 3, etc. Thus, the 3-nodes contact element stiffness matrix is

$$\mathbf{K}_3 = \mathbf{H}^T \mathbf{K}_{global} \mathbf{H} = \begin{bmatrix} S_n^2 \mathbf{K} & -S_n \mathbf{K} & S_n S_m \mathbf{K} \\ -S_n \mathbf{K} & \mathbf{K} & -S_m \mathbf{K} \\ S_n S_m \mathbf{K} & -S_m \mathbf{K} & S_m^2 \mathbf{K} \end{bmatrix} \tag{6}$$

2.2. Evaluation of unknown points

Figure 1 shows an active segment of the node-to-cubic-spline contact element during two time (force) steps and two iterations. All of the nodes in the Figure have been updated by adding the displacement of the last iteration. The coordinates of nodes C_{n+1} and D_{n+1} are unknown to be calculated at the current iteration. Since point C_{n+1} is on the cubic spline, eqn (7) can be obtained.

$$ax_c^3 + bx_c^2 + cx_c + d = y_c \tag{7}$$

where a, b, c and d are the coefficients of the cubic spline at segment 1–3. x_c and y_c are the x and y coordinates of point C_{n+1}. The eqn of length $|\overline{2_{n+1}C_{n+1}}|$ is

$$|\overline{2_{n+1}C_{n+1}}|^2 = (x_c - x_2)^2 + (y_c - y_2)^2 = (x_c - x_2)^2 + (ax_c^3 + bx_c^2 + cx_c + d - y_2)^2 \tag{8}$$

Where x_2 and y_2 are the x and y coordinates of point 2_{n+1}. Vector $2_{n+1} - C_{n+1}$ is perpendicular to the tangent direction of the cubic spline, and this means that length $|\overline{2_{n+1}C_{n+1}}|$ is relative maximum or minimum, so we obtain

$$\frac{\partial |\overline{2_{n+1}C_{n+1}}|^2}{\partial x_c} = 2(x_c - x_2) + 2(ax_c^3 + bx_c^2 + cx_c + d - y_2)(3ax_c^2 + 2bx_c + c) = 0 \tag{9}$$

The Newton–Raphson method may be applied to eqn (9) for finding x_c, and y_c is calculated from eqn (7). The coordinates of point D_{n+1} are evaluated by solving the two line eqns, line 1–3 and line $2_{n+1} - C_{n+1}$.

2.3. Internal forces of the contact element

From Fig. 1, the tangent displacement ΔU between the present force step and last force step is approximated to

$$\Delta U = (S_0 - S_n) L_{1-3} \tag{10}$$

where

$$S_0 = \frac{L_{D_0-3}}{L_{1-3}}, \quad S_n = \frac{L_{D_{n+1}-3}}{L_{1-3}}.$$

The total normal displacement V^* are approximate to

$$V^* = \overline{C_{n+1}2_{n+1}} \cdot (-v) \tag{11}$$

where $\overline{C_{n+1}2_{n+1}}$ means vector $C_{n+1}2_{n+1}$, and $\cdot$ means vector dot. If V^* is smaller than zero, the

node 2 has been separated from the target surface (Fig. 1); thus, the penalty constant and internal forces of the contact element are set to zero. If V^* is larger than zero, the internal forces of the contact node are first assumed to be fixed and can be obtained as follows:

$$F_n = kV^* \tag{12}$$

$$F_s = k\Delta U + (\mathbf{u_1} \cdot \mathbf{u})F_{s1} \text{ for stick} \tag{13}$$

where k is the penalty constant, F_{s1} is the internal shear force of the previous time step, and $\mathbf{u}_1$ is the tangent direction at the current node in the previous time (force) step. If $|F_s|$ of eqn (13) is larger than $|\mu F_n|$, the sliding mode should be set to get the internal forces as follows:

$$F_s = \mu F_n \quad \text{for sliding} \tag{14}$$

2.4. Validation of the node-to-cubic-spline contact element in bolted-joint analyses

The node-to-cubic-spline contact element was enhanced from the node-to-line contact element (Stone, 1992; Ju et al., 1995), which was validated by comparing a number of theoretical and bolted-joint analyses in these two references. Moreover, the SIFs of cracked bolted joints using this contact element were also compared with those using theoretical and experimental analyses (Ju, 1997a). Figure 2 shows a cubic-spline contact element with five target nodes, while the contact node can slide along or touch any point of the 5-node cubic spline. Since these target nodes are modeled by a cubic spline with continuous normal and tangent directions, the contact node slides across target nodes smoothly. This node-to-cubic-spline model, therefore, avoids the oscillations or the jump in the contact solution. Moreover, a very fine mesh near the contact surface is not necessary. A comparison of the contact stresses calculated by the theoretical analysis (Hyer et al., 1985) and the node-to-cubic-spline contact analysis for an infinite plate with a central bolted joint was performed. The geometry used in the finite element analysis is a square plate with the dimensions of $W/d_{hole} = 16.67$, where W is the plate width and d_{hole} is the hole diameter. The clearance ratio $((d_{hole} - d_{pin})/d_{hole})$ is set to 0.02, and the frictional coefficient is set to 0.2. Material

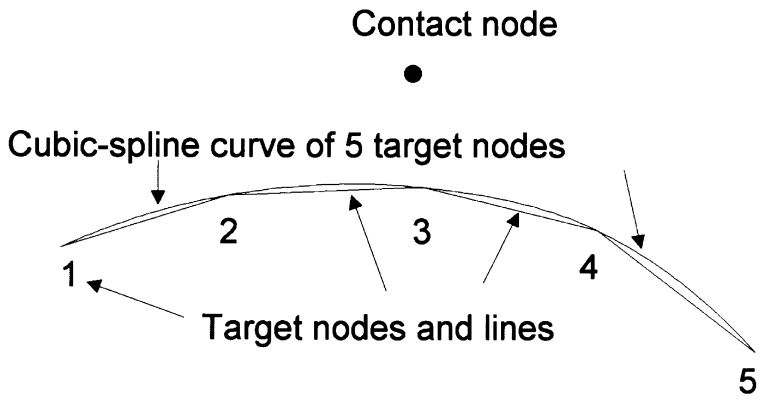

Fig. 2. 5-node cubic-spline contact element. (The number of target nodes is obtained from the input of the computer program.)

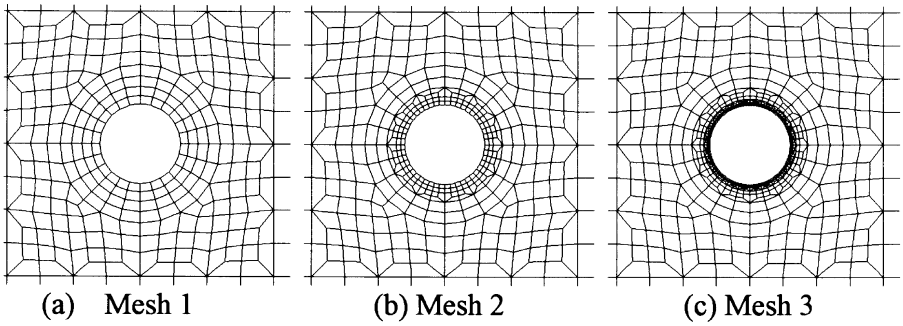

Fig. 3. Finite element meshes near the hole.

properties of the model are $E_x = 12.4$, $E_y = 3.73$, $G_{xy} = 3.21$ and $v_{xy} = 0.66$, where the units are ignored for convenience. The applied stress is 0.05 along the right edge of the square plate, and it is divided into 20 incremental force steps in the finite element analysis. Three FEM meshes from fine to coarse are shown in Fig. 3, in which 8-node quadrilateral plane-stress elements and 7-node node-to-cubic-spline contact elements are used. The comparisons are shown in Fig. 4, which indicates that the cubic-spline contact analyses are accurate and independent of the meshes. More

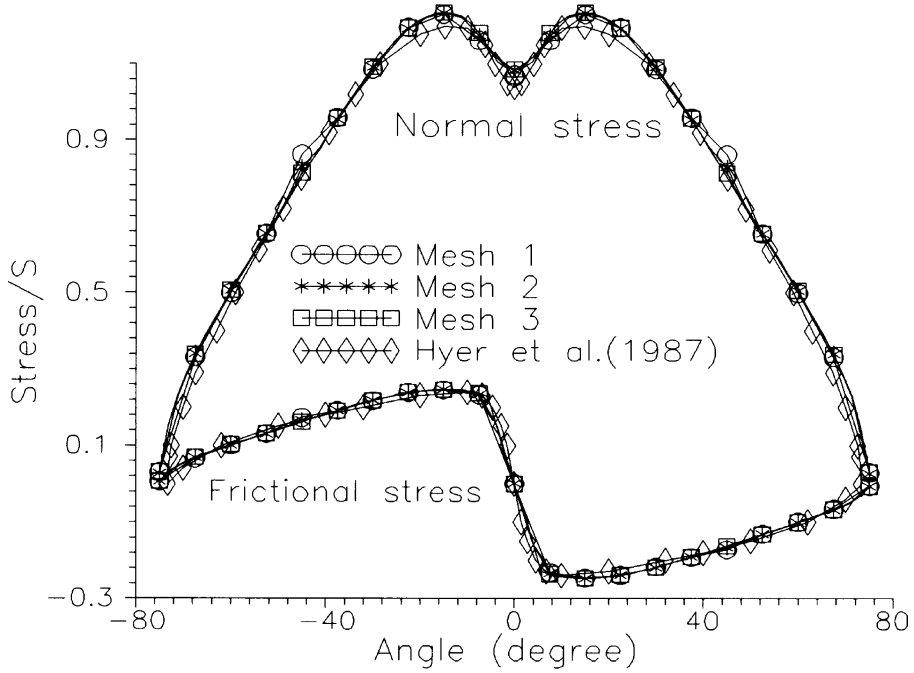

Fig. 4. Finite element results and theoretical solution from Hyer et al. (1987). (The stresses were directly obtained from the contact elements without any smoothing.)

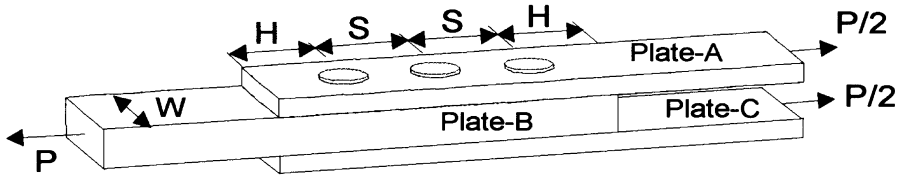

Fig. 5. Illustration of the model with three bolted joints.

validations can be found in Ju's report (Ju, 1998), which can be obtained from the Internet 140.116.36.221.

3. Numerical simulations of cracked bolted joints

3.1. Model illustration

The finite element model is a double-lapped rectangular plate with 1–4 bolted joints (Fig. 5) for fixed plate dimensions of the end distance $H = 50$ mm, the bolt spacing $S = 30$ mm, the plate width $W = 50$ mm and the hole diameter $d_{\text{hole}} = 10$ mm (hole radius $r = 5$ mm), where a single horizontal crack is located at one of the bolted joints in plate-B. The crack length ratio $(2(a+r)/W)$ is set to 0.2 (no crack), 0.20262, 0.225, 0.248, 0.29, 0.5 and 0.71. Figure 6 shows the plate-B of the models studied in this paper, where C11, C21, ..., C44 are the model names. The pins are assumed to be rigid. Since the joints are double lapped and rigid, the out-of-plane bending into the system is minor and neglected, so the analyses can be two-dimensional. A rigid-link scheme from reference (Griffin, 1994; Ju, 1997b) is used to model the flexible laps and rigid pins. In this scheme, plate-A and plate-C in Fig. 5 are modeled together as a single lap with the appropriate thickness. Plate-B with a single crack is modeled as another single lap with the appropriate thickness. The rigid circular pin is modeled as a master node and a number of slaved nodes, where the master node is set at the pin center and the slaved nodes are set on the boundary of the circular pin. All the displacements of the slaved nodes are the same as the master node under the assumption of no rotation of the pin. Thus, only two degrees of freedom, X-translation and Y-translation, are included at the rigid pin center. Then, the contact elements connect the slaved nodes of pins and the nodes along the holes of the laps.

Numerical simulations were performed by using eight-node quadrilateral and six-node triangular isoparametric elements and five-node node-to-cubic-spline contact elements in the plane-stress finite element analyses (FEA). Quarter-point-singular isoparametric elements (Henshell and Shaw, 1975; Barsoum, 1976) were also used around the crack tip. The linear elastic material properties used in the numerical analyses are listed in Table 1. Figure 7 shows a typical finite element model, in which a horizontal crack is located at the bottom hole. The total number of degrees of freedom varies between 20,000–76,000. The total stress P on the joint is applied numerically in 20 equal force steps. At the initial condition, the contact area is assumed at the bottom of the pin and hole, so only two nodes are touched together for the case with clearance ($d_{\text{hole}} > d_{\text{pin}}$; d_{hole} and d_{pin} are the hole and pin diameters). Under this condition the analysis is unstable if the static force-controlled loading is applied. For this reason, a vertical displacement of 0.002 mm is set at the

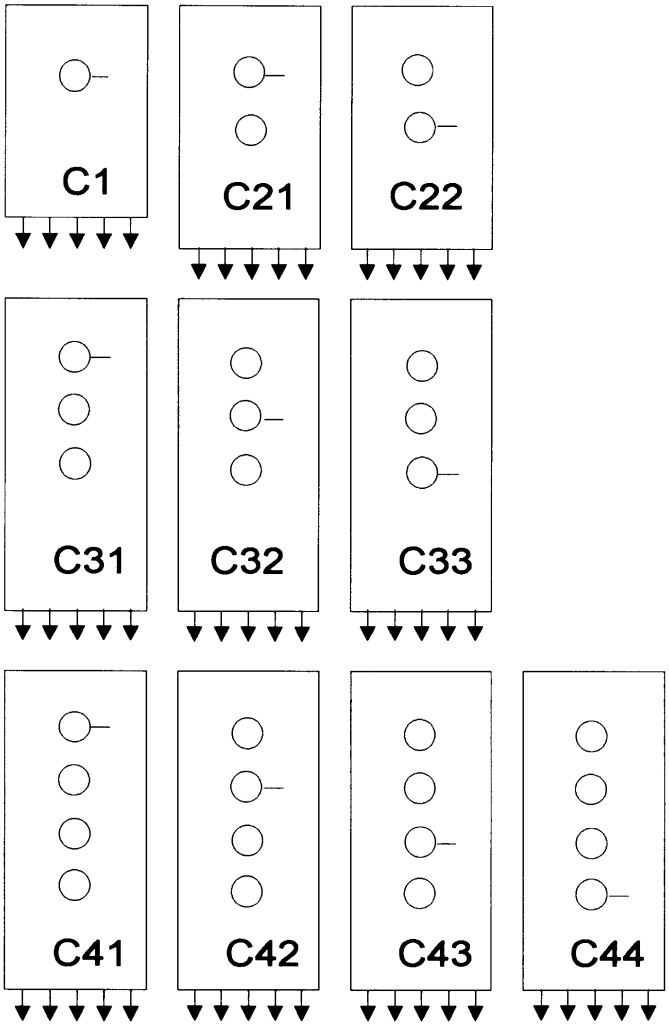

Fig. 6. The plate-B and its name of the finite element models.

Table 1
Material properties

Materials	E_{xx} (GPa)	E_{yy} (GPa)	v_{xy}	G_{xy} (GPa)
Aluminum	68.950	68.950	0.250	27.580
Boron epoxy	55.317	276.097	0.278	32.888
Sitka-Spruce wood	15.550	0.830	0.500	0.990

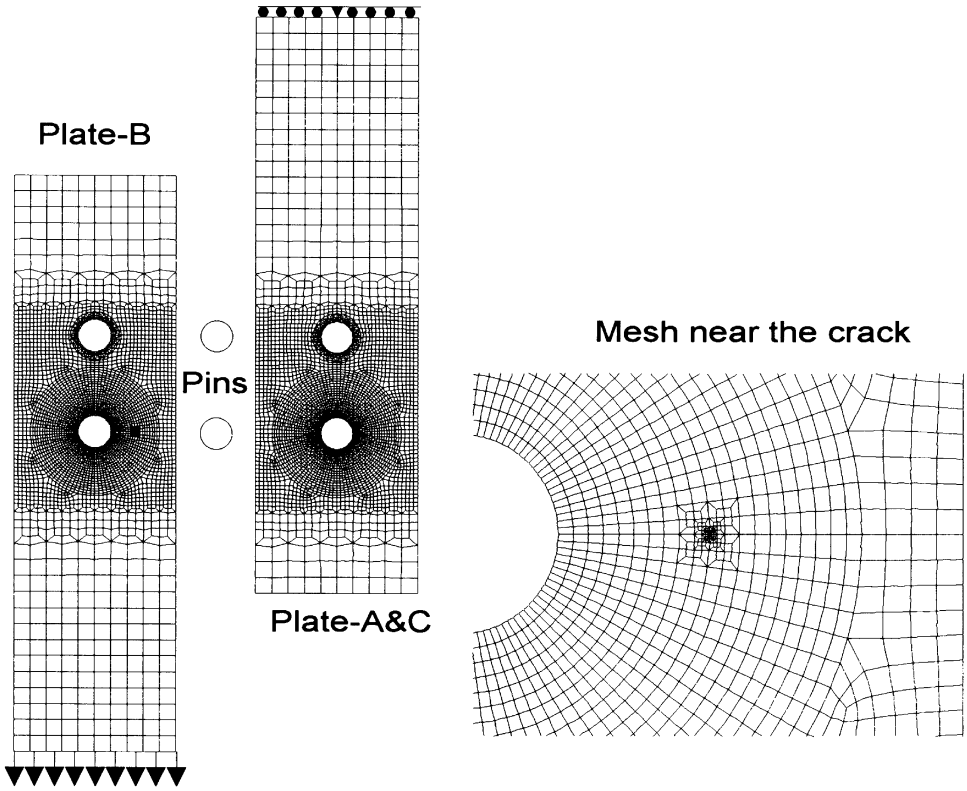

Fig. 7. A typical finite element mesh of a single crack in two-joint structure (Plate B, plate A & C and two pins are overlapped together. This figure shows them separate for reasons of clarity.)

bottom surface of the plate-B as the first force step, after which the 20 equal force increments are applied. Hence, there are a total of 21 force steps. The material is always assumed in the linear elastic range. Ju (1997a) indicated that reasonable changes in applied loading, friction and clearance do not significantly influence the K_I for pin-loaded joints. Thus, the finite element analyses use a clearance ratio of 0.01 and the frictional coefficient of 0.3 in this study; furthermore, only the SIFs of the maximum applied tension (the last force step) is calculated.

The least-squares method (Ju, 1996) is used to determine the SIFs of cracks. Ju (1997a) indicated that using K_I of the horizontal crack as the maximum opening-crack mode is sufficiently accurate even though the pure opening mode for cracked bolted-joint structures does not occur at this crack direction. Since the K_{II} of the horizontal crack is small for this horizontal crack, calculation of K_{II} is omitted in this paper.

3.2. Load ratios of pins

For multiple bolted-joint structures, the load supported by each pin can be different; thus, the load ratio of each pin is investigated in this study. The load ratio is defined as the load of the pin

over the total applied load. Figure 8 shows these pin load ratios at the cracked hole for isotropic material, Boron-Expoxy and Sitka-Spruce wood. These results indicate the following features.

(1) Although the properties of the three materials are very different, the figures of the load ratio vs normalized crack length are very similar to each other. This indicates that the load ratios are not sensitive to the material properties.
(2) When the normalized crack length increases, the load ratio decreases almost linearly; furthermore, each line in Fig. 5 is nearly parallel with a small slope. The averaged slope (S) of these lines in Fig. 5 is equal to -0.0654. This small slope indicates that the pin can still support the major part of the original loading at the uncrack condition when the crack propagates.
(3) When the crack length is equal to zero for the double-lap connection studied in this paper, the averaged load ratios from the three materials are listed in Table 2, where C21–C44 mean the name of the pin containing a dash (or a crack but crack length is equal to zero) shown in Fig. 3. This table exhibits that the external pins support more loading than the internal pins.

From Table 2 and the averaged slope ($S = -0.0654$ in this study), eqn (15) can be used to estimate the load ratio of the pin at a certain crack length.

$$R = R_0 - S(L - L_0) \tag{15}$$

where R is the load ratio of the pin at the normalized crack length of L, R_0 is the load ratio without crack, and can be obtained from Table 2, L is the normalized crack length for the load ratio R, L_0 is equal to $(2r)/W$.

The accuracy of eqn (15) is studied here, and first the error is defined as the difference of the load ratios from eqn (15) and FEA over the load ratio from FEA. The maximum error of all the load ratios calculated from the three materials is 13% and the averaged error is 2.9%. Thus, a simple equation can be used to estimate the load ratio reasonably.

3.3. SIFs of a single crack in multiple joints

The mode-I SIFs were then calculated by using the least-squares method (Ju, 1996), in which the maximum radius to include the displacement data was set to 90% of the crack length, and the number of the displacement terms is set to 8. Each material contains ten cases shown in Fig. 3, and each case contains five different crack lengths. Thus, 50 mode-I SIFs can be obtained for each material, and these calculated mode-I SIFs K_I were normalized into the non-dimensional stress intensity factors Ke_I according to the eqn (16). Since P and r in eqn (16) are constant for all the least-squares analyses in this study, one can compare the magnitude of these normalized SIFs changing with crack lengths directly.

$$Ke_I = \frac{K_I}{P\sqrt{\pi r}} \tag{16}$$

where $r = d_{hole}/2$ is the radius of the hole; P is the applied tension at the bottom surface of the plate-B.

These normalized mode-I SIFs were shown in Fig. 5, which indicate the following features:

(1) For four-pin structures the sequence from the largest value to the smallest value of the mode-

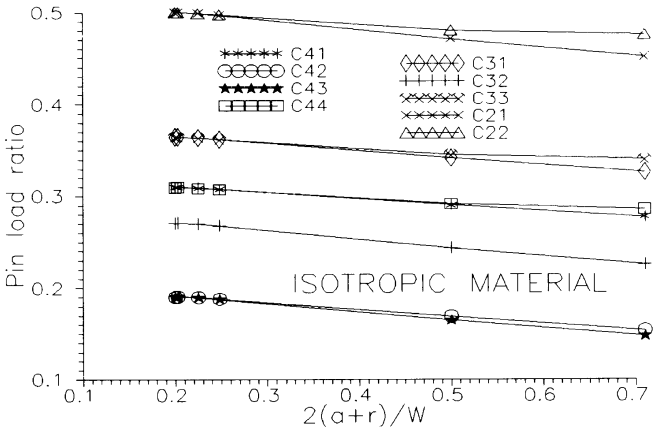

(a) Isotropic material

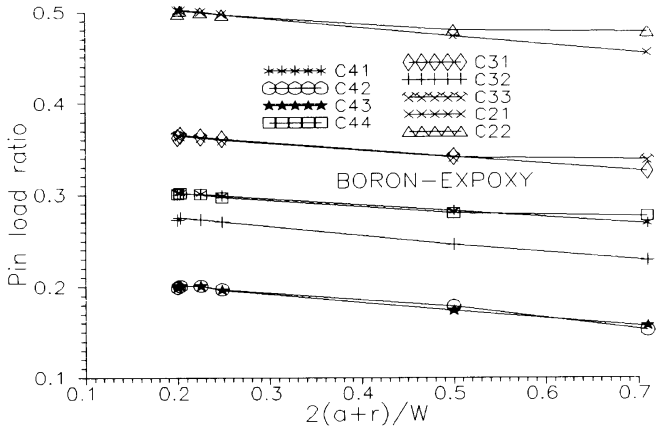

(b) Boron-Expoxy

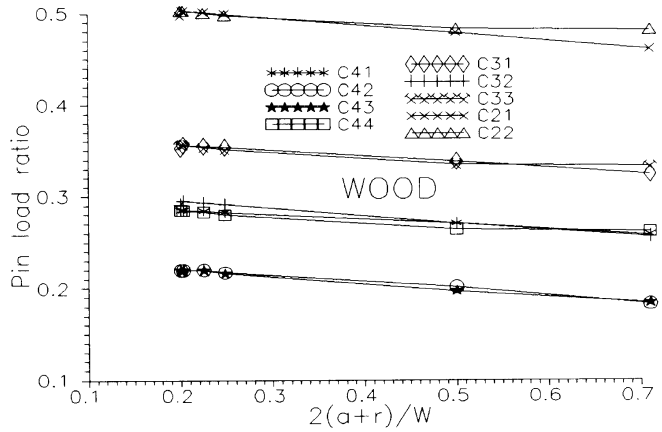

(c) Sitka-Spruce wood

Fig. 8. Load ratio of pins.

Table 2
Load ratio of the uncracked double-lapped connection

Pin	C21 and C22	C31 and C33	C32	C41 and C44	C42 and C43
Load ratio (%)	50	36	28	30	20

I SIFs is C44, C43, C42 and C41, for three-pin structures the sequence is C33, C32 and C31, and for two-pin structures the sequence is C22 and C21. These sequences exhibit that the cracked hole which is closer to the applied force is more critical. Especially for the hole closest to the applied force (the first hole), its mode-I SIF is much larger than others. Thus, the failure of the multiple bolted-joint structures should be first at this hole.

(2) The mode-I SIFs of the cases of C44, C33 and C22 are very similar. The reason is probably that the applied force dominates the stress field of the first hole. This situation cannot be overcome by the arrangement of more pins in the plate, since the critical condition of the first hole will change little when the number of pins increases.

(3) Except the cases of C11 and C41, the mode-I SIF increases when the crack grows. This condition indicates that the critical condition of the cracked hole will not reduce when the crack propagates. This situation can be very serious, since other uncracked holes give little help to this cracked hole even for a large crack length. Especially for the first hole, it sustains the largest pin load and the largest mode-I SIF, which are reduced little for crack propagation. Furthermore, the break from the first hole will cause the plate disconnected from the joint.

Figure 9 shows that the distribution of SIFs is complex for different locations of the crack. This condition is not convenient for practice; therefore, an equivalent applied force (P_e) is investigated to normalize the SIFs in order to obtain a regular distribution of the SIFs for different locations of the crack (Fig. 6). A residual value (*Res*) is defined in eqn (17) at a certain crack length for the ten cases in Fig. 6.

$$Res = \sum_{i=1}^{10} \left(\frac{K_{I_i}}{P_e \sqrt{\pi a_e}} - K_{eff} \right)^2 \tag{17}$$

where i means one of the crack location in Fig. 4. K_{I_i} is the mode-I SIF for the case i, a_e is the normalized crack length ($= 2(a+r)/W$), K_{eff} is the equivalent SIF at a certain crack length.

Defining the formula of P_e and minimizing the residual value in eqn (17), one can find the constants in the formula of P_e. The stress field near the crack tip should be highly influenced by the net applied force (P_n), the sustained force of this cracked hole (P_c) and the sustained force of the hole in the front of this cracked hole (P_f). The net applied force can be obtained using the total applied force minus all the sustained forces of the holes in front of this cracked hole. After trial and error, eqn (18) was found to be an appropriate formula for this equivalent applied force.

$$P_e = P_n + (\alpha P_c + \beta P_f)/a_e^2 \tag{18}$$

where α and β are two constants dependent of material and geometry. The two values can be

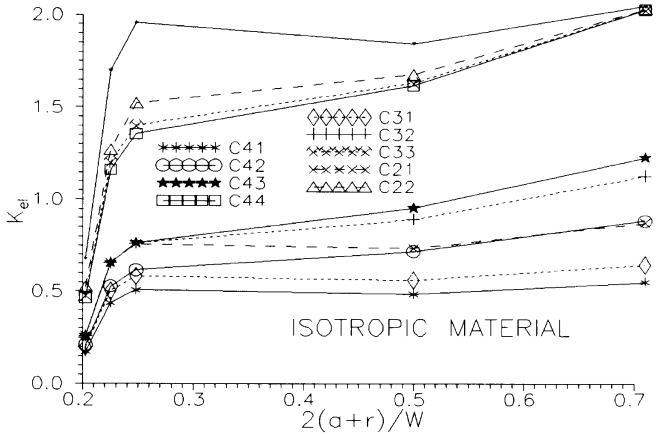

(a) Isotropic material

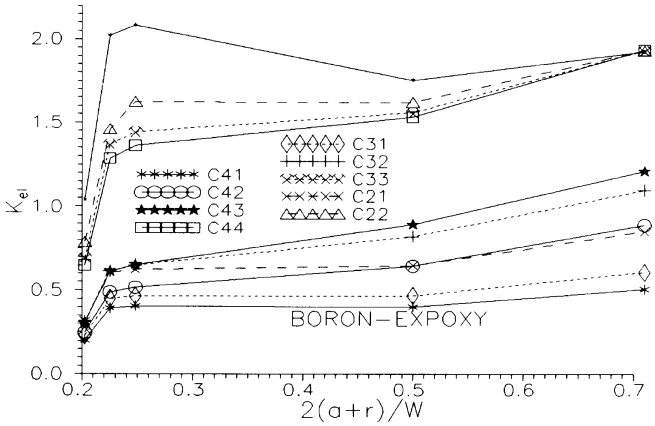

(b) Boron-Expoxy

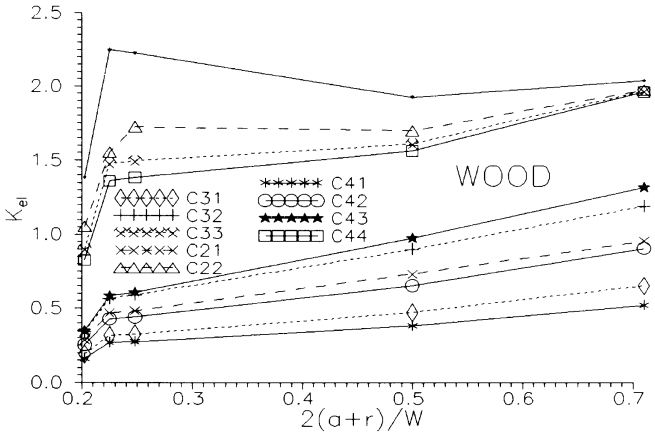

(c)Sitka-Spruce wood

Fig. 9. The value Ke_{I} vs normalized crack length.

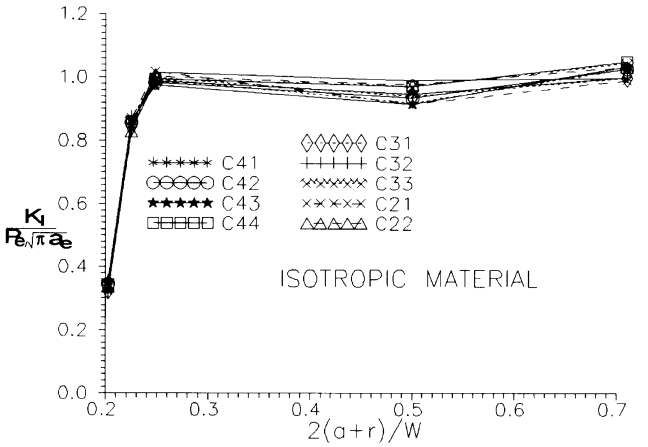

(a) Isotropic material

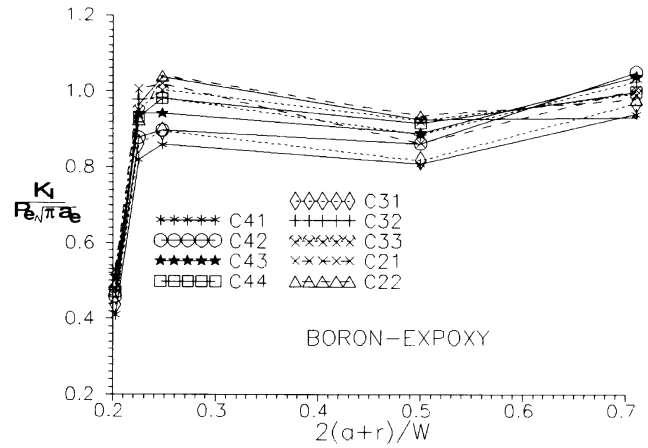

(b) Boron-Expoxy

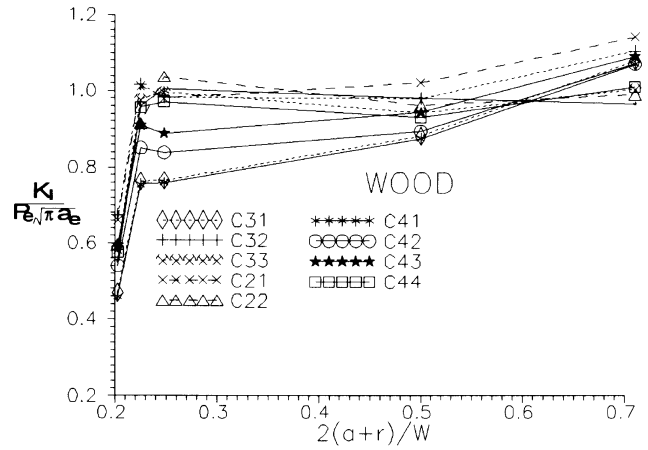

(c) Sitka-Spruce wood

Fig. 10. The value $K_I/P_e\sqrt{\pi a_e}$ vs normalized crack length.

Table 3
α and β for the three materials

Material type	α	β
Aluminum	0.0450	−0.0235
Boron-Epoxy	0.0495	−0.0425
Sitka-Spruce wood	0.0610	−0.0680

obtained by using the least-squares scheme, or an alternative in this paper is designing a computer program to find the two constants by changing α and β little by little, and choose one pair of α and β that can minimize eqn (17). Table 3 shows these α and β for the three materials.

Figure 10 shows the normalized SIFs by using P_e. For isotropic material, the distribution of the normalized SIFs can be very regular; moreover, the normalized SIFs approach to one for the a_e larger than 2.5. For anisotropic materials, the distributions are not so regular as that of the isotropic material, but they are still much better than these in Fig. 9.

4. Summary

(1) The load ratios of the loaded pins are not sensitive to the material properties. Moreover, the pin can still support the major part of the original loading at the uncracked condition when the crack propagates.
(2) For the multiple bolted-joints structure, the first hole sustains the largest pin load and the largest mode-I SIF, which are reduced little for crack propagation. This critical condition cannot be reduced by the arrangement of more pins in the plate, since the SIF of the crack near the first hole will be changed little when the number of pin is increased.
(3) Two simple formulae can be used to fit the load ratios and SIFs of the multiple bolted-joints problems within reasonable accuracy.

Acknowledgement

This study was supported by the National Science Council, Republic of China, under contract number: NSC-86-2213-E-006-063. An executable compressed file in MS-DOS can be obtained using the ftp server, and the procedures are listed below:

ftp 140.116.36.221 (login name: **ftp** and password: **[Enter]**)
binary
get nfemnew.exe

This file contains the manual and the FORTRAN source codes of a nonlinear finite element program (Ju, 1998), where source file SCONT.FOR includes the cubic-spline contact element.

References

Barsoum, R.S., 1976. On the use of isoparametric finite elements in linear fracture mechanics. International Journal of Numerical Methods in Engineering 10, 25–38.

Cartwright, D.J., Ratcliffe, G.A., 1972. Strain energy release rate for Radial cracks emanating from a pin-loaded hole. International Journal of Fracture Mechanics 8, 175–181.

Cartwright, D.J., Parker, A.P., 1982. Opening mode stress intensity factor for cracks in pin-loads joints. International Journal of Fracture 18, 65–78.

Chiang, Y.J., Rowlands, R.E., 1991. Finite element analysis of mixed-mode fracture of bolted composite joints. Journal of Composites Technology & Research, JCTRER 13, 227–235.

Griffin, O.H. Jr, Hyer, M.W., Cohen, D., Shuart, M.J., Yalamanchili, S.R., Prasad, C.B., 1994. Analysis of multifastener composite joints. Journal of Spacecraft and Rockets 31, 278–284.

Henshell, R.D., Shaw, K.G., 1975. Crack tip elements are unnecessary. International Journal of Fracture Mechanics 9, 495–509.

Hong, C.S., Chu, S.J., 1982. Stress intensity factor force cracks emanating from pin-loaded hole by photoelastic method. In: Proceedings of the Joint SESA–JSME Meeting, pp. 612–617.

Hsu, T.M., 1981. Analysis of cracks at attachment lugs. Journal of Aircraft 18, 755–760.

Hyer, M.W., Klang, E.C., 1985. Contact stresses in pin-loaded orthotropic plates. International Journal of Solids and Structures 21, 957–975.

Ju, S.H., 1996. Simulating stress intensity factors for anisotropic materials by the least-squares method. International Journal of Fracture 81, 283–297.

Ju, S.H., 1997a. Stress intensity factors for cracks in bolted joints. International Journal of Fracture 84, 129–141.

Ju, S.H., 1997b. Investigating contact stresses on articular surfaces by 3-D rigid links. Journal of Engineering Mechanics, ASCE, 123, 1253–1259.

Ju, S.H., 1998. Development of a nonlinear finite element program with rigid link and contact element. Report of NSC in R.O.C., NSC-86-2213-E-006-063, 66–81.

Ju, S.H., Stone, J.J., Rowlands, R.E., 1995. A new symmetric contact element stiffness matrix for frictional contact problems. Computer & Structure 54, 289–301.

Kirkby, W.T., Rooke, D.P., 1977. A fracture mechanics study of residual strength of pin lug specimens. In: Fracture Mechanics in Engineering Practice. Applied Science, London.

Liu, A.F., Kan, H.P., 1977. Test and analysis of cracked lug attachments. Int. Conf. on Fracture (ICF4), Canada, 3, pp. 656–664.

Narayana, K.B., Dayananda, T.S., Dattaguru, B., Ramamurthy, T.S., Vijayakumar, K., 1994. Cracks emanating from pin-loaded lugs. Engineering Fracture Mechanics 47, 29–38.

Rahman, M.U., Rowlands, R.E., 1993. Finite element analysis of multiple-bolted joints in orthotropic plates. Computers and Structures 46, 859–867.

Smith, C.W., Jolles, M., Peters, W.H., 1979. Stress intensities for cracks emanating from pin-loaded holes. In: Flaw Growth and Fracture, ASTM STP 631, pp. 190–201.

Stone, J.J., 1992. Experimental-numerical analysis of bolted joints in finite composites with and without inserts. Ph.D. thesis, University of Wisconsin-Madison.